

Quantitative trait locus mapping and transcriptome analysis reveal candidate genes for a stem bending mutant in rapeseed (*Brassica napus*)

Mengna Yu^a, Rui Zhang^a, Yajun Liu^b, Yuan Gu^b, Guoxia Shang^c, Yonghai Fan^a, Miao Liu^a, Shengting Li^a, Yuqiao Tang^a, Chuanfang Wan^a, Xuli Wu^a, Cunmin Qu^{a,d,e}, Jiana Li^{a,d,e}, Kun Lu^{a,d,e,*1}

^a College of Agronomy and Biotechnology, Southwest University, Beibei, Chongqing 400715, China

^b Agricultural Technology Extension Station in Lincang City, Lincang 677000, China

^c Academy of Agricultural and Forestry Sciences, Qinghai University, Xining 810016, China

^d Academy of Agricultural Sciences, Southwest University, Chongqing 400715, China

^e Engineering Research Center of South Upland Agriculture, Ministry of Education, Chongqing 400715, China



ARTICLE INFO

Keywords:

Brassica napus
Stem bending
Quantitative trait locus
Transcriptome
Polar auxin transport

ABSTRACT

Rapeseed is one of the most important oilseeds crops worldwide. Although stem development greatly affects crop yield, its molecular mechanisms remain elusive in rapeseed. This study found a *stem bending 1* (*stb1*) mutant in rapeseed with abnormal stem development and performed phenotype characterization, genetic analysis, quantitative trait locus mapping, and transcriptome analysis. The key stage of stem bending in *stb1* mutant occurred at Biologische Bundesanstalt, Bundessortenamt and CHemical industry (BBCH) stages 59–61, from the end of stem elongation to early flowering. The number of vessels and the degree of development of stem xylem, sclerenchyma, and parenchyma cells were extremely lower in *stb1* mutant than in elite cultivar ZS11. Genetic analysis revealed that *stb1* is controlled by a single recessive locus located between markers Bn-A01-p2421445 and Bn-A01-p4230829 on chromosome A01. Using RNA-seq, identified 1631 genes that differentially expressed between mutant and normal F₂ plants in the shoot apical meristem and stem. The down-regulated genes were mainly overrepresented in auxin transport and coenzyme metabolism processes. Combining data on the auxin concentrations in stem and expression of candidate genes within the mapping interval in the mutant, it was speculated that the phenotype of the *stb1* mutant may be caused by defects in polar auxin transport, as two auxin transport-related genes were obviously down-regulated in the mutant. Among them, *BnSOS3-INTERACTING PROTEIN3*, which encodes a CBL-interacting protein kinase, was considered the most promising candidate gene for further investigation. These results lay a foundation for better understanding the molecular mechanisms of stem development in rapeseed.

1. Introduction

The plant stem provides mechanical support to the leaves, flowers, and fruit, and connects the shoot with the root system (Zheng et al., 2018). As the main vascular organ, it is also responsible for transport of

water and mineral nutrients, remobilization of photosynthates from vegetative to reproductive organs, and transduction of long-distance signals within the plant body. As a storage organ, the stem accumulates starch and proteins in underground storage stems in potato (*Solanum tuberosum*), and photosynthates in the aboveground main stem in

Abbreviations: *stb1*, stem bending 1; PAT, polar auxin transport; *SIP3*, *SOS3-INTERACTING PROTEIN3*; *PIN*, *PIN-FORMED*; *PILS*, *PIN-LIKES*; QTL, quantitative trait locus; BBCH, Biologische Bundesanstalt, Bundessortenamt and CHemical industry; PH, plant height; SN, siliques numbers; BN, ranch number; SEM, scanning electron microscopy; IAA, indole-3-acetic acid; SNP, single nucleotide polymorphism; LOD, logarithm of odds; MAFs, minor allele frequencies; cM, centimorgans; SAM, shoot apical meristem; IS, internal stems; ES, external stems; RNA-seq, RNA sequencing; FPKM, fragments per kilobase per million mapped; DEGs, differentially expressed genes; FDR, false discovery rate; GO, gene ontology; qRT-PCR, quantitative real-time PCR; BS, bending site; ABS, above bending site; BBS, below bending site; GC-MS, Gas chromatography - mass spectrometry; CWR, Cell Wall Residues; *ARF16*, Auxin response factor 16.

* Corresponding author at: College of Agronomy and Biotechnology, Southwest University, Beibei, Chongqing 400715, China.

E-mail address: drlukun@swu.edu.cn (K. Lu).

¹ ORCID: 0000-0003-1370-8633.

<https://doi.org/10.1016/j.indcrop.2021.114456>

Received 9 August 2021; Received in revised form 8 October 2021; Accepted 22 December 2021

Available online 29 December 2021

0926-6690/© 2021 Elsevier B.V. All rights reserved.

maize (*Zea mays*) and rapeseed. Hence, plant stems play crucial roles in yield in many crops. For example, the selection of shorter and more robust stems conferred by semi-dwarf mutations resulted in the development of many high-yielding crop varieties, and doubling of grain yields over the last 50 years (Khush, 2001). Interestingly, in spite of its roles in crop yield, the molecular mechanisms controlling stem development and phenotype variation remain largely unexplored.

Stem development mutations, such as bent stems, lead to a reduction of mechanical support and increased risk of lodging (falling over) (Peng et al., 1999), which inevitably result in yield losses and increased cost and difficulty of mechanized harvesting. Several stem bending mutants have been identified in *Arabidopsis* (Kato et al., 2002), maize (Multani et al., 2003), rice (*Oryza sativa*) (Wu et al., 2015), tomato (*Solanum lycopersicum*) (Pnueli et al., 1998), and *Populus* (Williams et al., 2015). Functional characterization revealed that the stem bending-related genes are involved in at least three kinds of molecular mechanisms: the gravity response, hormone response, and vascular development regulatory pathways (Zheng et al., 2018). In *Arabidopsis*, the *sgr4/zig* mutation reduced SNARE complex formation and hindered polar auxin transport (PAT), disrupting membrane trafficking between the *trans*-Golgi network and the vacuole, and causing abnormalities in shoot gravitropism and morphology (Hashiguchi et al., 2010; Kato et al., 2002). The maize *br2* mutation is caused by loss of P-glycoprotein in the ABCB1 auxin transporter that modulates PAT in the stalk, which is essential for normal stalk development and architecture (Multani et al., 2003; Pilu et al., 2007). These studies indicate that PAT may be one of the determining factors associated with the stem bending phenotype in plants, and is worth further investigation in other crops.

After auxin is synthesized in the apical meristem (Ljung et al., 2001), it is transported through the parenchyma cells in the xylem along the main stem to the base of the stem (Friml, 2003). PAT regulates the distribution of auxin in different parts of the plant and involves the uneven distribution of auxin carriers on cell membranes, which forms an auxin concentration gradient (Friml, 2003; Zheng et al., 2018). PAT occurs by action of auxin uptake transporters of the AUXIN RESISTANT1/LIKE AUX (AUX/LAX) family, and auxin efflux transporters of the ATP-Binding Cassette subfamily B/P-glycoprotein (ABCB/MDR/PGP) and the PIN-FORMED (PIN) family (Habets and Offringa, 2014; Kaneda et al., 2011; Swarup and Peret, 2012). The PIN-LIKES (PILS) transport facilitator family also regulates intracellular auxin homeostasis in plants (Barbez et al., 2012).

PAT in stems is particularly reduced in *pin1* mutants (Geldner et al., 2001; Noh et al., 2003), and *Arabidopsis pin1* mutants show similar phenotypes to wild-type plants treated with auxin transport inhibitors (Galweiler et al., 1998), indicating that *PIN1* plays an important role in PAT. The growth of *pin2* and *pin3* mutants showed that *PIN2* is associated with auxin distribution and root growth (Abas et al., 2006), and *PIN3* is related to plant growth and phototropic growth (Benkova et al., 2003). However, not all PAT mutants display a stem bending phenotype. Hence, it is necessary to identify more stem bending mutants to unravel the molecular mechanisms of PAT in relation to the stem bending trait.

Rapeseed is one of the most important oilseed crops worldwide, and artificial breeding strategies have substantially improved its yield. Consequently, the pod canopy of modern cultivars is noticeably thicker than that of landraces, placing an increased burden on the stem. To better understand the molecular mechanisms of stem development, this study identified a *stem bending 1* (*stb1*) mutant in rapeseed. Compared the phenotype and physiological traits between the *stb1* mutant and the elite cultivar ZS11, and combined the results of genetic analysis, quantitative trait locus (QTL) mapping, and transcriptomic comparison to identify candidate genes regulating the stem bending trait in rapeseed. These results provide valuable insight into the molecular mechanisms controlling stem development and will aid breeding programs to improve stem strength and thus reduce the risk of yield loss due to lodging in rapeseed.

2. Materials and methods

2.1. Plant materials

Using an F₂ segregating rapeseed population consisting of 273 individuals derived from a cross between the *stb1* mutant and cultivar 'Zhongshuang 11' (ZS11) to map QTLs for the stem bending mutation. The female parent *stb1* was selected from a recombinant inbred line in an advanced generation of 'GH06×ZY821', and was selfed for 6 consecutive generations, with stable phenotypic inheritance of the bending stem trait at BBCH stage 60 (first flower open) (Lancashire et al., 1991). The male parent ZS11 is a conventional, high-quality rapeseed variety bred by the Institute of Oil Crops, Chinese Academy of Agricultural Sciences. The F₂ individuals together with the two parental lines were grown in Beibei, Chongqing, China (29°45' N, 106°22' E, 238.57 m above sea level) in 2014. A total of 273F_{2:3} lines derived from an F₂ population were selected, and 20 plants per F_{2:3} family were grown in Beibei in 2015. All seeds were sown at the end of September and transplanted to the field one month later, as previously described (Lu et al., 2016). All lines were planted in a randomized complete-block design with three replications. Each plot contained 3 rows with 10 plants per row, 20 cm between plants within each row, and 30 cm between rows.

2.2. Trait evaluation

To compare the agronomic trait differences between the *stb1* mutant and the elite cultivar ZS11, the plant height (PH), stem angle, siliques number (SN), branch number (BN), and number of seeds per silique after harvest were assessed.

2.3. Vascular tissue staining

Samples for histochemical staining were taken from the *stb1* mutant and ZS11 at the initial flowering stage, and three replicates were used for each material and all materials had approximately the same stem parts (Fig. 1a). Stems were cut into 2 cm pieces and fixed in embedding liquid. A Thermo Scientific HM525 NX microtome was used to cut cross-sections of the material. In brief, 1% phloroglucinol solution and 36% hydrochloric acid were used as chromogenic reagent. After staining, the samples were washed off with pure water 3 times and photographed under a Nikon ci-L microscope. ImageJ software (National Institute of Health, USA) was used to calculate the cell size and cell number per unit area (Liu et al., 2021).

2.4. Scanning electron microscopy observation

The cellular morphology of the vascular tissue was observed using a scanning electron microscope(SEM) SU3500 (Hitachi, Tokyo, Japan) with the following parameters: temperature – 20 °C, voltage 5000 V, and magnification 200× (Lima et al., 2019). Three biological replicates were used for each sample.

2.5. Determination of IAA content

The concentrations of the auxin indole-3-acetic acid (IAA) were assayed in the abovementioned samples using a commercial Plant IAA ELISA Kit (Bluegene Co. Ltd., Shanghai) and a microplate reader (DNM-9602, CANY Tec, Shanghai).

2.6. Determination of lignin monomer content

The lignin polymer in the stems of the *stb1* mutant, ZS11, and F₁ plants was lysed by the alkali nitrobenzene oxidation method using 65 mg of stem powder (passed through a 40-mesh sieve). The samples were placed in benzene-ethanol (67/33, V/V) solution in a Soxhlet

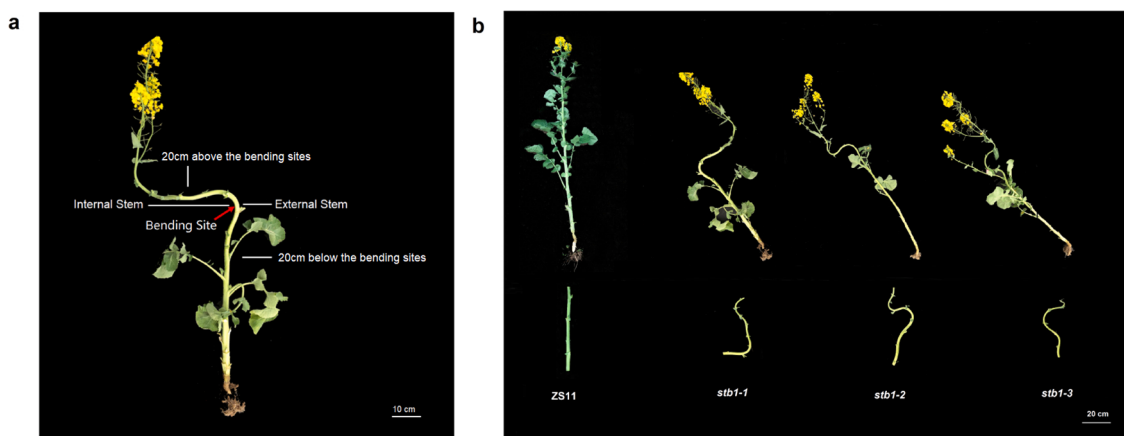


Fig. 1. The phenotype of the elite cultivar ZS11 and the *stb1* mutant at the initial flowering stage. (a): The stem of *stb1* mutant showing the IS and ES, 20 cm above the bending site, and 20 cm below the bending site. ES: External stem; IS: Internal stem. Scale bars, 10 cm. (b): The whole-plant phenotype of ZS11 and the *stb1* mutants grown in the field showing a straight stem in ZS11 and bent stems in the *stb1* mutants. The stem bending of the *stb1* mutants mainly occurs above the middle of the stem. Scale bars, 25 cm.

extractor and extracted for 4 h at 100 °C, then air-dried in a fume hood to a constant weight. The measurement of lignin polymer was carried out according to the ROLANDO method (Rolando et al., 1992).

2.7. Genotyping and *Brassica* 60 K SNP Bead Chip Array analysis

Genomic DNA was extracted from the parental lines and the F₂ individuals using the CTAB method (Lu et al., 2008). Genotyping was conducted using the *Brassica* 60 K Illumina Infinium single nucleotide polymorphism (SNP) array (Illumina Inc., San Diego, CA) as described in the manufacturer's protocol. The genetic linkage map composed of genome-wide SNPs was constructed using JoinMap 4.0 software (Stam, 1993), with a minimum logarithm of odds (LOD) score of 2.5. The SNP data were analyzed using WinQTL Cartographer 2.5 (Wang et al., 2006). SNPs with minor allele frequencies (MAFs) of < 0.05 or lacking a call higher than 0.9 were excluded from analysis, as previously described (Lu et al., 2016). The physical localization of SNPs was determined using a BLASTN search against the *B. napus* reference genome v4.1 (Chalhoub et al., 2014), with an E-value cut-off of 1E-5. Final genetic distances in centiMorgans (cM) were calculated from recombinant frequencies using the Kosambi mapping function and Mapmaker v3 software (Lander et al., 1987). Composite interval mapping was conducted to detect the QTLs associated with the stem bending trait by WinQTL Cartographer 2.5 with default parameters. After 1000 permutation tests, a locus with an LOD threshold value was regarded as potential QTL. The LOD confidence intervals surrounding the peak of the QTL likelihood plot were considered as the QTL intervals for candidate gene screening. At the same time, Haplovview software (Barrett et al., 2005) was used for haplotype analysis.

2.8. Transcriptional analysis of the candidate genes

The shoot apical meristem (SAM) was harvested from 15F₂ lines with the stem bending phenotype and 15F₂ lines without the stem bending trait at BBCH stage 55 (individual flower buds on the main inflorescence visible but still closed), and pooled as two transcriptomic comparison bulks (denoted as SAM-m (for mutant) and SAM-w (for wide type)). Total RNAs of samples were isolated using EZ-10 DNAaway RNA Mini-Prep Kit (Sangon Biotech, Shanghai, Co., Ltd.). Equimolar concentrations of total RNA from 15F₂ lines were pooled together to form four extreme RNA bulks (two pooled samples with two biological replicates). At BBCH stage 61, RNAs of plants with bent stems, internal stem (IS, the side of the stem with the smaller angle) and external stem (ES, the side of the stem with the larger angle) (Fig. 1a) and corresponding normal

stems at the same position were also sampled and pooled (denoted as Stem-mIS, Stem-mES, and Stem-w, respectively). Equimolar concentrations of total RNA from 15F₂ lines were pooled together to form six extreme RNA bulks (three pooled samples with two biological replicates).

Library construction and RNA sequencing (RNA-seq) were conducted on an Illumina HiSeq 2500 platform (Illumina, San Diego, California, USA) (Niu et al., 2020) by the Novogene Technologies Corporation (Beijing, China). Raw sequencing reads were filtered using Fastp (Chen et al., 2018), and the clean data were mapped to the *Brassica napus* reference genome v4.1 (<https://www.genoscope.cns.fr/brassicanapus/>) using STAR v2.5.3 (Dobin et al., 2013). Gene counts data were generated by featureCounts (Yang et al., 2014). Differentially expressed genes (DEGs) were detected using DESeq2 R package (Love et al., 2014) with the following criteria: absolute fold change > 2 and false discovery rate (FDR) < 0.05.

The gene ontology (GO) enrichment of the DEGs was explored using topGO, and R package ggplot2 (Ginestet, 2011) was used to produce the figure. The website KOBAS 3.0 (<http://bioinfo.org/kobas/>) was used for KEGG pathway enrichment analysis (Bu et al., 2021). The raw sequence data reported in this paper have been deposited in the Genome Sequence Archive (Genomics, Proteomics & Bioinformatics 2017) in National Genomics Data Center (Nucleic Acids Res 2021), China National Center for Bioinformation/Beijing Institute of Genomics, Chinese Academy of Sciences, under bioproject accession number PRJCA006781 and are publicly accessible at <https://ngdc.cncb.ac.cn/>.

2.9. qRT-PCR validation

To validate the accuracy of the transcriptomic data and expression variation of the differentially expressed candidate genes, 17 independent cDNA samples were obtained and subjected to quantitative real-time PCR (qRT-PCR) analysis. cDNA was synthesized from the elite cultivar (ZS11) and the *stb1* mutant and used for RNA-seq using PrimeScript RT Master Mix Kit (TaKaRa, Dalian, China). The primers were obtained from qPrimerDB (<https://biodb.swu.edu.cn/qprimerdb>) (Lu et al., 2018) (Table S1). *Actin7* was used as the internal standard for normalizing the qRT-PCR results. The relative expression levels were calculated using the 2^{-ΔΔCt} method.

2.10. Statistical analysis

SPSS v20.0 was used for statistical analysis with one-way analysis of variance (ANOVA); results are expressed as mean ± standard error and

t-test of significance. *, $P < 0.05$; **, $P < 0.01$. The results were presented using GraphPad Prism 8.0 software (GraphPad Software, California, USA). The data were presented as means \pm standard errors (Liu et al., 2021).

3. Results

3.1. Morphology of the stem bending mutant

Observations in the field showed that the stem bending trait of the *stb1* mutant occurred between 10 days before flowering to 5 days after flowering, which means that the crucial period for the stem bending phenotype occurred between the BBCH stages 59–61. The stem then resumed normal upright growth at the later stages. The bent sites of the stem were mainly located at a height of 1.0–1.5 m from the soil (Fig. 1b).

The agronomic traits of the *stb1* mutant at the harvesting stage were investigated. Compared with the elite cultivar ZS11, the plant height of the *stb1* mutant was significantly reduced ($P = 0.005$) from 209.5 to 166.5 cm, but its branch number and pod number were not changed. The average seed number per siliques decreased significantly (from 27.7 to 9.9, $P = 0.002$), as did the average siliques length (from 10.4 to 3.4, $P = 0.002$), leading to a significant yield loss. These trait variations may be due to the bending of the *stb1* mutant stem, resulting in a decrease of plant height and therefore decreased photosynthesis efficiency and carbohydrate accumulation, which further affect siliques development and biomass accumulation (Table S2).

3.2. Cytological observation of the *stb1* mutant

To observe the stem structure in the *stb1* mutant, three parts of the stems from the *stb1* mutant and ZS11 at the early flowering stage were sampled: the bending site (BS), and 20 cm above (ABS) and below (BBS) the bending site as shown in Fig. 1a. The stem cross-sections were stained with phloroglucinol to detect vascular tissue system, and the staining results are shown in Fig. 2a, which showed that the stem is mainly composed of phloem, xylem, vascular cambium, and pith. In addition, the staining results also indicated that the areas of xylem, vessels, thick-walled tissues, and parenchyma cells around the xylem at the BS, ABS, and BBS were all significantly reduced ($P = 0.02$). The statistical analysis revealed that the staining area ratio of the vascular tissue of the bent stem of the *stb1* mutant was extremely lower than that of ZS11 (Fig. S1), which is consistent with the vascular tissue staining of the stem.

Next, the difference of the staining area ratio between the IS and the ES of the *stb1* mutant was compared. The stained area ratio of the IS and the number of xylem and surrounding parenchyma cells was extremely lower than that of the ES (Fig. S1). Hence the bending phenotype of the *stb1* mutant may be related to an underdeveloped vascular system. That is, the vascular system of the IS responsible for PAT is not as developed as that of the ES. When auxin is transported, the PAT rate on the external side of the stem would be rapid, and the stem would bend toward the relatively underdeveloped side of the vascular system.

Observation of cross-sections by SEM showed that the xylem and surrounding parenchyma cells, vessels, and other vascular tissues were not as developed in the *stb1* mutant as in ZS11, and the parenchyma cells of the mutant were loosely arranged (Fig. 2b). The parenchyma cells in

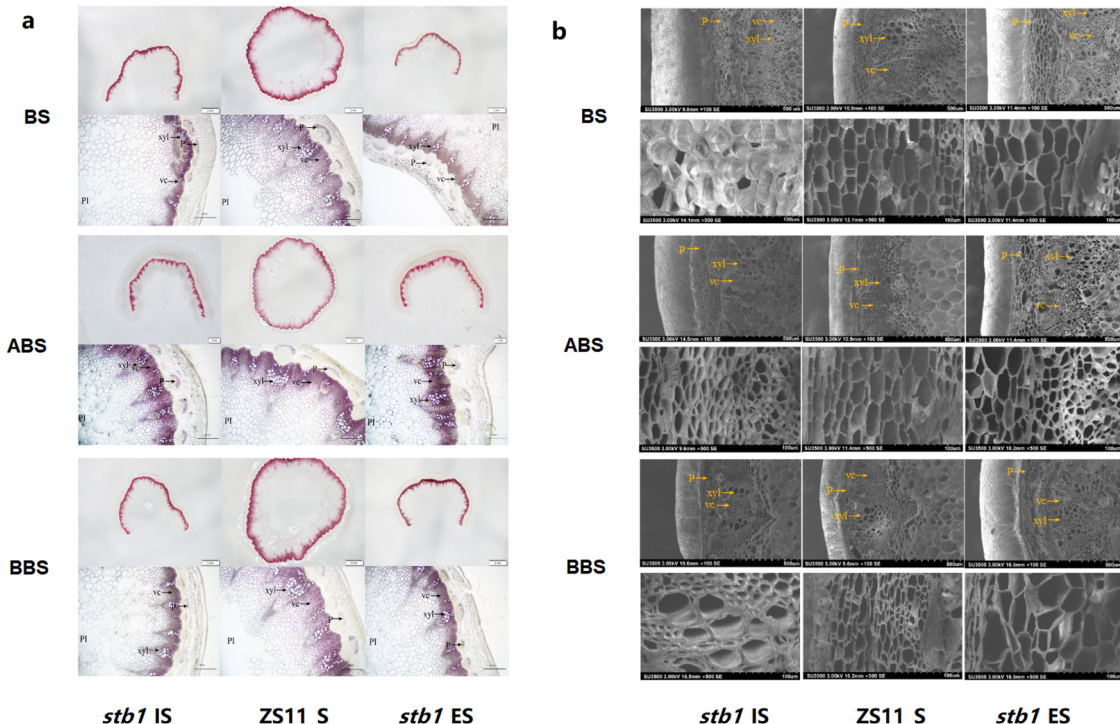


Fig. 2. Vascular tissue staining and SEM of vascular tissue in stems of ZS11 and the *stb1* mutant at the early flowering stage. (a): Phloroglucinol staining of vascular tissue in stem tissues in the elite cultivar ZS11 and the *stb1* mutant. Histochemical staining indicated that the xylem, vessels, and parenchyma cells in the *stb1* mutant stem were less developed than those of the elite cultivar ZS11. Compared with the ES, the number of xylem and parenchyma cells of the IS were reduced. PI: pulp; P: phloem; vc: vascular cambium; Xyl: xylem. Scale bars, 2 mm (above), 100 μ m (below); BS: the bending site; ABS: 20 cm above the bending site; BBS: 20 cm above the bending site; S: stem; ES: External stem; IS: Internal stem. (b): SEM observation of stems in ZS11 and the *stb1* mutant. The xylem and the surrounding parenchyma cells, ducts, and other vascular tissues in the stalk of the mutant were not as well developed as those in ZS11, and the parenchyma cells of the mutant were loosely arranged. Generally, the xylem of the IS was more developed than that of the ES, while the vascular tissues of the ES were more developed than those of the IS. Compared with the inner parenchyma cells, the shape of the cells of the ES of the mutant was irregular, and the intercellular space was larger. Scale bars, 500 μ m (above), 100 μ m (below). BS: Bending site; ABS: 20 cm above the bending site; BBS: 20 cm above the bending site; S: stem; ES: External stem; IS: Internal stem.

the ES were characterized by irregular shapes and larger intercellular spaces compared with the IS. In summary, the xylem of the IS was less developed than that of the ES in the mutant. The SEM results were consistent with those from the vascular tissue staining, and both indicate that the stem bending phenotype is caused by underdeveloped internal vascular tissue and inconsistent development of the IS and ES in the *stb1* mutant.

3.3. Comparison of lignin monomers and auxin content

To understand the role of *STB1* in the lignin biosynthesis pathway, gas chromatography-mass spectrometry (GC-MS) was used to determine the content of three kinds of lignin monomers in the stems (Fig. 3a). In the elite cultivar, the content of S and G lignin in ZS11 was 228.96 $\mu\text{mol/g}$ cell wall residue (CWR) and 157.24 $\mu\text{mol/g}$ CWR, respectively, and the S/G lignin ratio was 1.45. The content of S and G lignin of the *stb1* mutant was 188.78 $\mu\text{mol/g}$ CWR and 92.18 $\mu\text{mol/g}$ CWR, respectively, and the S/G lignin ratio was 2.05, which is obviously higher than that of ZS11. The H lignin content in these plants was very small, less than 0.2% of the total lignin content. Also, the accumulation of lignin monomers in 15F₁ lines was analyzed. The content of S and G lignin monomers in F₁ plants averaged 180.35 $\mu\text{mol/g}$ CWR and 109.08 $\mu\text{mol/g}$ CWR, respectively. The total lignin content between the *stb1* mutant and the F₁ plants was similar, but their stem bending phenotypes differed; hence, the stem bending phenotype may not be related to lignin content.

The content of the IAA was measured in the IS and ES of the *stb1* mutant and the ZS11 stem at the late bolting and early flowering stages. The $R^2 = 0.9909$ of the regression equation ($y = -0.0367 + 0.189x$) (Fig. S2) suggested that the experimental error was well-controlled in our measurement. The detailed values for standard curves are shown in the Table S3. The IAA content of the *stb1* mutant showed an upward trend from the late bolting stage to the early flowering stage (Fig. 3b). The content of auxin in the IS was lower than that in the ES at the late bolting stage ($P = 0.04$), while the reverse trend was observed at the early flowering stage. These results suggest that auxin transport may be affected at the bending site of the mutant. The difference of auxin concentration from the late bolting to the early flowering stages could lead to different growth rates between the IS and ES in the elongation zone in the mutant, eventually causing the stem to bend.

3.4. Genetic analysis of the *stb1* mutant

The F₁ individuals from reciprocal crosses of the *stb1* mutant and

ZS11 all showed a normal stem phenotype, implying that the stem bending phenotype is controlled by a recessive gene (Fig. 4a). To analyze the genetic mechanism underlying the *stb1* mutation, the 273 individuals in the F₂ population were examined, and the differences in the degree of stem bending among the plants were found (Fig. 4a). A total of 215 and 58 plants showed normal and bent stems in the F₂ population, respectively. The phenotypic separation ratio was about 3:1 (Table S4), and the Chi square test value was $\chi^2 = 2.05 < \chi^2_{(0.05)} = 3.84$, suggesting that the *stb1* mutation might be segregating in accordance with Mendelian autosomal recessive single gene inheritance. Then, the F₁ with ZS11 and the *stb1* mutant was backcrossed, and the segregation ratio was about 1:1, which further confirmed that the stem bending phenotype is controlled by a single recessive gene.

3.5. Linkage map construction and QTL mapping

Among the F₂ segregating individuals, we extracted genomic DNA from 40 bent and 71 normal plants, as well as the two parents, for genotyping based on the *Brassica* 60 K chip array. Of the 52,157 SNPs, 47,139 SNPs were detected within more than 110 samples, implying that the SNP chip hybridization was successful and suitable for subsequent analysis. A total of 16,159 SNPs showed differences between ZS11 and the *stb1* mutant, and 11,721 SNPs without obvious separation were used to construct genetic linkage map by using MSTMap (<http://mstmap.org>). After removing the repeated loci, a genetic linkage map containing 20 linkage groups (Table 1) was generated, including 1799 SNPs, covering 1821.72 cM with an average distance of 0.99 cM using Joinmap 4.0 (Fig S3). The single marker SNP analysis conducted by WinQTL cartographer 2.5 mapped *STB1* on chromosome A01, between markers Bn-A01-p2421445 and Bn-A01-p4230829, with a genetic distance of 1.802 cM (Fig. 4b). BLASTN analysis of all SNP markers within the mapping interval against the *B. napus* genome revealed that the distance is 1.995 Mb, located 1911995–3907633 on chromosome A01.

SNP markers on A01 were compared with the genome sequence of *Brassica napus* published in France by BLASTN to determine the physical position of SNP markers on the genome. Then, the linkage disequilibrium analysis of 40 SNPs on A01 chromosome was performed using Haploview 4.2. The parameters were set as $R^2 \geq 0.8$, D' = 1, and LOD value ≥ 3 . The results showed that there were 6 haplotype segments on chromosome A01, with sizes of 19, 232, 425, 114, 346 and 298 KB, respectively, including 23 SNP markers (Fig. 4c). Block-a01-2 and Block-A01-3 with the highest significance were very consistent with the location obtained according to the genetic linkage map (Table S5).

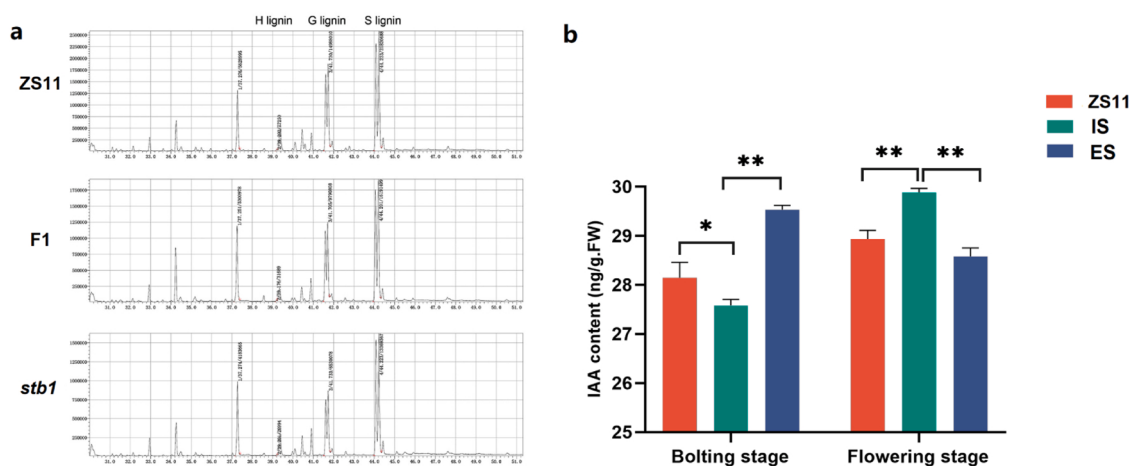


Fig. 3. The content of lignin monomers and auxin in ZS11 and *stb1* stems. (a): The determination of stem monolignols in ZS11, the *stb1* mutant, and F₁ plants by GC-MS in the early flowering stage. (b): The auxin content in ZS11 and *stb1* stems in the late bolting and early flowering stages. The content of auxin in the IS during the bolting stage was lower than that in the ES, while the content of auxin in the IS during the early flowering stage was obviously higher than that in the ES. Data are means (\pm SD) of three repeats. ES: External stem; IS: Internal stem. Student's t-test, ** represents $P < 0.01$.

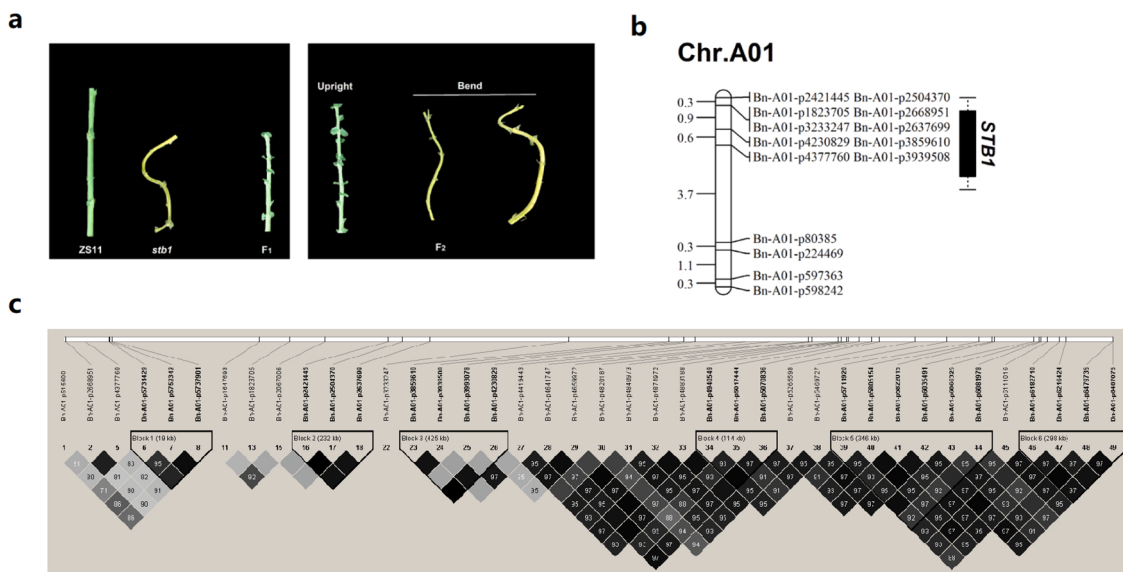


Fig. 4. Candidate gene interval prediction based on single marker SNP locus. (a): The stem phenotype of ZS11, the *stb1* mutant, and F₁ and F₂ individuals in the flowering stage; (b): Preliminary mapping of *STB1*. BLASTN analysis of all SNP markers within the interval against the *B. napus* genome sequences revealed that the distance between Bn-A01-p2421445 and Bn-A01-p4230829 on chromosome A01 is 1.995 Mb. Numbers on the left indicate the map distance (cM) and names on the right indicate the marker with the physical distance (bp). (c) The linkage disequilibrium analysis among various SNPs locus on A01 chromosome.

Table 1
Summary statistics of the linkage map for *B. napus*.

Chr	Marker number	Genetic distance (cM)	Average distance between loci (cM)	Max spacing (cM)
A01	127	130.87	1.04	15.37
A02	72	85.65	1.21	10.07
A03	167	112.37	0.68	14.37
A04	25	24.18	1.01	13.70
A05	153	114.47	0.75	13.01
A06	106	87.33	0.83	8.41
A07	132	93.58	0.71	5.45
A08	113	68.67	0.61	2.68
A09-1 ^a	66	60.47	0.93	6.51
A09-2 ^b	84	96.25	1.16	17.60
A10	84	75.84	0.91	11.24
C01	76	95.00	1.29	16.54
C02	81	80.71	1.00	18.75
C03	109	108.45	1.00	13.20
C04	78	93.78	1.20	5.27
C05	55	104.79	1.91	19.99
C06	61	105.90	1.74	18.97
C07	112	111.32	0.99	9.77
C08	40	66.60	1.67	8.81
C09	58	92.47	1.59	17.69
A	1129	949.67	0.85	17.60
C	670	859.01	1.29	19.99
Total	1799	1808.68	1.01	19.99
(A+C)				

A09-1^a: one linkage for chromosome A09.

A09-2^b: another linkage for chromosome A09.

3.6. Identification of differentially expressed genes between the two extreme pools

To reveal gene expression patterns and transcriptional regulation in the *stb1* mutant, transcriptome sequencing was performed on 10 samples consisted of 5 pooled samples with two biological replicates. In total, more than 60 Gb of sequencing data were obtained with an average of 6 Gb data per sample. After filtering the low-quality reads, the GC content of all samples varied from 45.70% to 47.20%, and the range of Q30 was from 89.50% to 92.90%. Subsequently, clean reads were mapped to the reference genome, and the average unique mapping rate was reached to 86.11%, indicating that the sequencing quality was

suitable for further the differential expression analysis.

In order to determine the reliability of transcriptional sample replicates, we performed the correlation between two biological replicates, and we provided heatmap of the sample-to-sample distances and principal component plot of the samples (PCA) for evidence of high repeatability between replicates (Love et al., 2014). A heatmap of this distance matrix reflected the similarities and reliability of replicates (Fig. S4). Moreover, the results of hierarchical clustering showed that replicates for per sample were clustered together, and SAM and stem from same materials were also clustered (Fig. S5), respectively. Similarity with distance matrix, our PCA results illustrated the repeatability and reliability of replicates from the same sample. In addition, we supplemented qRT-PCR experiments for four genes to further examine the reliability of RNA-seq analysis results. The results showed that the expression levels of *IAA19* and *APR3* at SAM and stem in *stb1* were higher than those in ZS11, and the expression levels of *PIN1* and *CKL3* at SAM and stem of ZS11 were higher than those in *stb1* (Fig. S6). The qRT-PCR results were consistent with RNA-seq analysis, which further confirmed the reliability of RNA-seq analysis.

Through comparison between the two extreme pools, a total of 610 DEGs were identified in the SAM in the extreme pools, among which 82 genes were up-regulated and 528 genes were down-regulated. Additionally, a total of 1502 DEGs were identified in the stem (IS and ES) differential analysis, among which 567 genes were up-regulated and 935 genes were down-regulated. Using a Venn diagram, we identified 481 DEGs shared between the SAM and the stem (Fig S7).

Next, the functions of the DEGs in the SAM and stem of the *stb1* mutant were analyzed (Fig. 5a, Fig. S8). The up-regulated genes of the *stb1* mutant were mainly enriched in ‘response to ethylene-activated signaling pathway’ (GO:0009873), ‘plant-type hypersensitive response’ (GO:0009626), ‘ATP biosynthetic process’ (GO:0006754), and ‘response to organic substance’ (GO:0010033). Down-regulated genes were mainly overrepresented in ‘glycosyl compound metabolic process’ (GO:1901657), ‘auxin biosynthetic process’ (GO:0009851), ‘auxin polar transport’ (GO:0009926), ‘glucosinolate biosynthetic process’ (GO:0019758), and ‘organonitrogen compound metabolic process’ (GO:1901564). These findings suggest that several hormone regulation pathways are activated in the *stb1* mutant, especially the auxin regulation pathway, which indicates that the stem bending phenotype may be related to abnormal auxin biosynthesis and transport in the mutant.

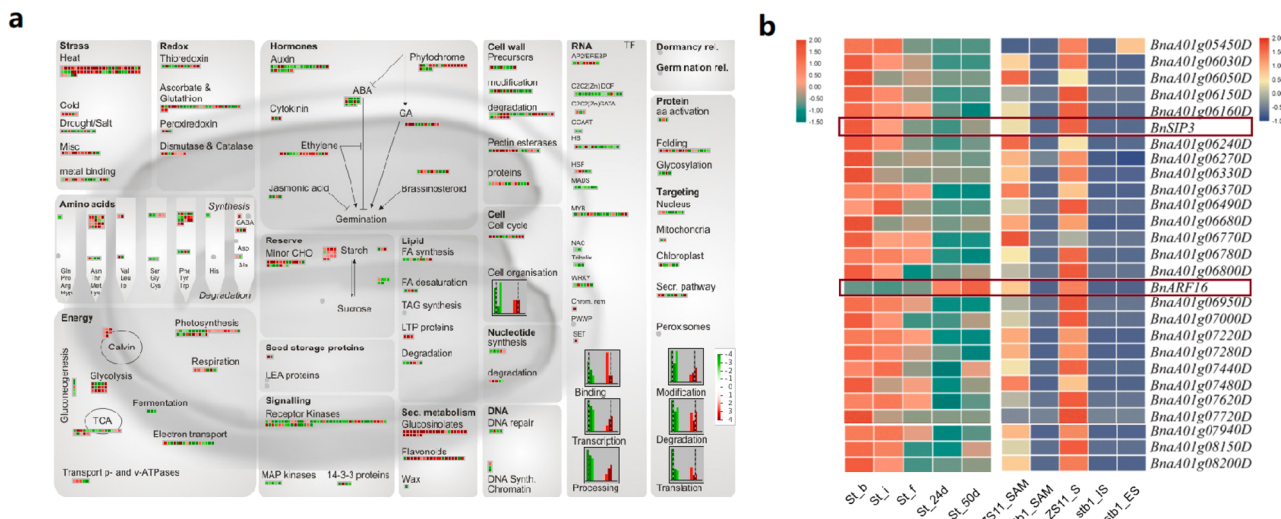


Fig. 5. Identification and functional enrichment analysis of DEGs. (a): The Mapman analysis of secondary metabolic pathways genes between ZS11 and *stb1* stem in early flowering stage Red for up-regulated genes, green for down-regulated genes. (b): Stem-specific expression profiles of candidate genes in the mapping interval in the elite cultivar ZS11 and the *stb1* mutant. Genes within the mapping interval were identified based on the SAM and stem RNA-seq data between the two extreme pools. The color bar at the upper right side of the figure represents Log₂(FPKM+1), red indicates high expression and blue indicates low expression. St_b: Stem at bud stage, St_i: Stem at first flowering period, St_f: Stem at full flowering period, St_24d: Stem at seed 24DAP, St_50d: Stem at seed 50DAP. ZS11_SAM: the shoot apical meristem of ZS11, *stb1*_SAM: the shoot apical meristem of *stb1*; ZS11_S: the stem of ZS11; *stb1*_IS: the internal stem of *stb1*; *stb1*_ES: the external stem of *stb1*.

Therefore, it was found that the synthesis and metabolism of auxin in this mutant were not inhibited, but the genes in the auxin transport pathway were obviously down-regulated. Based on this, this study speculated that the stem bending phenotype might be caused by abnormal PAT, leading to abnormal accumulation of auxin in the bent site in the mutant.

GO enrichment analysis of down-regulated genes in the *stb1* mutant identified 25 genes related to PAT. Among them, PILSs belong to a family of proteins that are similar to PIN auxin transporters: *PILS3* (*BnaC06g21810D*), *PILS1* (*BnaA06g14780D*), and *PILS5* (*BnaA06g14780D*) are involved in the synthesis of auxin efflux transporters; *ACUALIS 5* (*BnaC02g08800D*) affects stem internode elongation and vascular bundle development; *THALIANA V-PPASE1* (*BnaC06g40530D*) regulates the pH of the apoplast to affect the localization of auxin export proteins.

The KEGG metabolic pathway analysis showed that the DEGs were mainly enriched in 'plant hormone signal transduction', 'biosynthesis of other secondary metabolites', 'carbon metabolism', 'oxidative phosphorylation', and 'biosynthesis of amino acids' (Fig. S9). Multiple phytohormone signal transduction pathways are activated in the *stb1* mutant, which is in accordance with the results of GO enrichment analysis, further suggesting that the auxin content variation in the *stb1* mutant is likely to be related to abnormal auxin transport.

3.7. Identification and validation of candidate genes

To identify candidate genes involved in stem bending in the mutant, we combined the results of QTL mapping and transcriptome comparison. A total of 27 DEGs were detected in the Bn-A01-p2421445 and Bn-A01-p4230829 marker interval and the 200-kb flanking region in the SAM and stem between the two extreme pools. By analyzing the expression levels of the candidate genes within this interval at each stage of rapeseed growth (Fig. 5b), the expression of most DEGs was extremely higher in the stem at BBCH stages 59–61 than in the other stages of growth. Then the functions of the candidate genes were investigated by searching for their homologs in *Arabidopsis*, of which only two (all down-regulated in the mutant) were related to hormone synthesis, transport, and signal transduction. *BnARF16* (*Auxin response factor 16*, *BnaA01g06910D*) is involved in transport and signal transduction of

auxin; *BnSIP3* (or called *BnCIPK6*) (*BnaA01g06180D*) is involved in PAT (Tripathi et al., 2009). These two genes are the most likely candidate genes for *stb1*.

To further validate the three candidate genes, qRT-PCR was used to compare their expression patterns in the roots, stems, leaves, flowers, and siliques between ZS11 and the *stb1* mutant at the early flowering stage. The expression levels of *BnSIP3* and *BnARF16* were extremely lower in the mutant than in ZS11 (Fig. 6a). The qRT-PCR results were consistent with the RNA-seq analysis, confirming the reliability of the RNA-seq results. The expression of *BnARF16* was obviously lower in all tissues in the *stb1* mutant than in ZS11, except for in the root, while the expression of *BnSIP3* was extremely lower in all tissues investigated in the mutant than in ZS11. In addition, the expression levels of *BnARF16* at each stage of rapeseed growth (Fig. 5b), the expression was particularly lower in the stem at BBCH stages 59–61 than in the other stages of growth. This expression pattern contradicted previous guesses about the key stage of stem bending in *stb1* mutant. Based on the gene functional annotation and expression patterns in the mutant, *BnSIP3* seems the most promising candidate gene, followed by *BnARF16*, and deserve further investigation to unravel the molecular mechanisms of stem development in rapeseed.

4. Discussion

Plants that exhibit stem bending generally show reduced plant height, and stems generally show shortened internodes and continuous bending, such as the *zig/sgr4* mutant of *Arabidopsis* and the *br2* mutant of maize (Kato et al., 2002; Multani et al., 2003). Since Kilen (Kilen and Hartwig, 1975) reported a soybean (*Glycine max*) stem bending mutant, mutants with abnormal stems have been investigated from a morphological (Walker and Boerma, 1978) and a genetic perspective (Boerma and Jones, 1978; Kilen, 1990). Soybean stem bending is influenced by photoperiod and light intensity, and stem development may be affected by changes in the level or distribution of endogenous hormones. The stem bending trait in the *stb1* mutant may also be related to altered endogenous hormone distribution.

Stem development is affected by various hormones such as auxin, brassinolide, and gibberellin. Among them, auxin stimulates xylem and phloem differentiation, cell expansion, and stem elongation, which

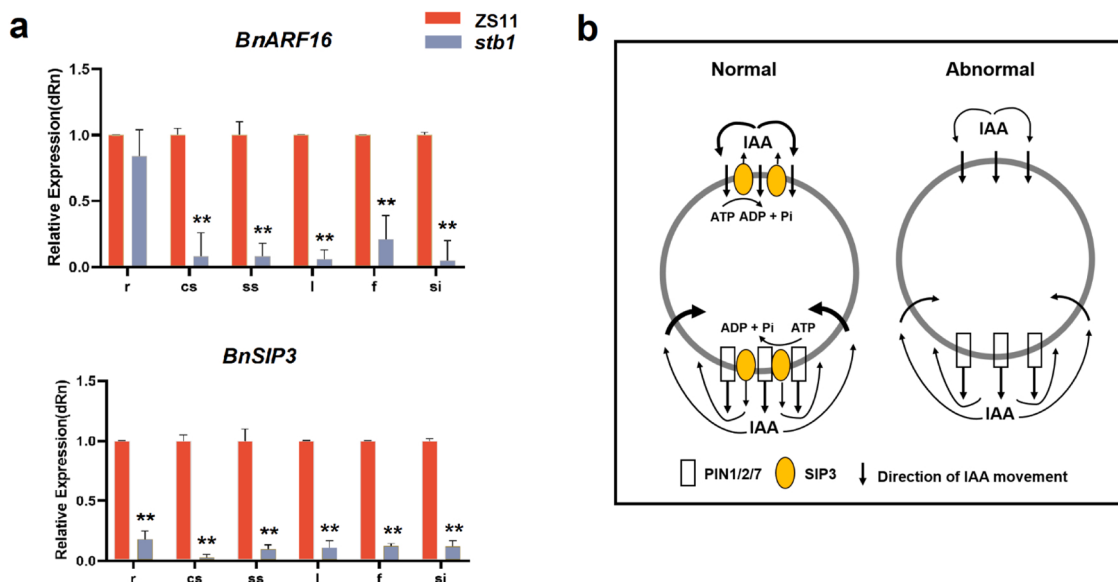


Fig. 6. Proposed molecular pathways in rapeseed connecting PAT to stem development. (a): Differential expression analysis of candidate genes in different tissues and organs between the elite cultivar ZS11 and the *stb1* mutant. r: root; cs: curved stem; ss: straight stem; f: flower; l: leaf; si: silicle; Student's *t*-test, * represents $P < 0.05$ and ** represents $P < 0.01$. (b): Model of auxin rediffusion in the normal and abnormal cell. The energy-dependent transport of auxin by CIPK6 increases the directionality of auxin transport. In normal meristematic regions, an energy-dependent transport mechanism is needed to overcome the localized high auxin concentration. When CIPK6 and PINs colocalize subcellularly, synergistic PIN–CIPK6 interactions lead to an increased rate and specificity of auxin transport and confer a directional bias to auxin movement. In abnormal *stb1* mutant cells, arrows indicate the direction and magnitude of auxin flux. IAA, indole-3-acetic acid.

plays an important role in plant growth and development. Auxin is mainly synthesized in young tissues such as stem meristems and young leaves (Ljung et al., 2001), and is then transported through the thin-walled cells located in the xylem. The development of vascular bundles affects auxin transport capacity. Auxin can induce the formation of continuous vascular bundles, and the development of vascular bundles is closely related to PAT. In this study, we stained the vascular tissues and found that the cells responsible for PAT in the *stb1* mutant were underdeveloped compared with those in ZS11. The vascular system responsible for PAT was less developed on the IS than on the ES; therefore, PAT is stronger in the ES, in which the auxin content is high. The stem then bends toward the relatively underdeveloped side. Further research on the *stb1* mutant will help reveal the relationship between vascular bundle development and PAT.

Since many factors affect stem elongation, including external light conditions, stem composition, gene regulation, and endogenous hormone levels, the regulation of stem development is very complicated. Auxin is an important hormone for plant growth and development. Due to the unique polar transportation mode of auxin, an auxin concentration gradient is produced in plant tissues and organs, which plays an important role in controlling the growth and development of plants, affecting apical dominance, vascular tissue differentiation, and plant tropism. PAT is mediated by the auxin import carrier AUX1/LAX, the auxin export carrier ABCB/PGP, and the PIN family (Barbosa et al., 2018; Bennett et al., 1996; Geisler et al., 2017; Hoyerova et al., 2018; Naramoto, 2017). PIN1 is mainly expressed in vascular tissues and the SAM, and plays a role in early embryonic development (Okada et al., 1991). PIN1 protein is located in the vascular tissue of plants and constitute the transcellular membrane component of the auxin export complex. If PIN1 activity is inhibited, the morphology of the stem is altered (Friml et al., 2002). Auxin in *Arabidopsis* is transported by PIN1 through the vascular tissue in a polar manner to the cell base. Therefore, the PIN family plays a role in controlling auxin efflux.

This study was identified 25 PAT-related genes among the down-regulated genes in the *stb1* mutant. These mainly include the auxin export carrier PIN family members PIN1 and PIN4, ACL5 (involved in the elongation of stem internodes and the development of vascular

bundles), and AVP1 (which regulates extracellular pH to influence auxin export protein localization). Within the marker interval of Bn-A01-p2421445 and Bn-A01-p4230829 marker and the 200-kb flanking sequence, including 27 DEGs in the SAM and stem between the two extreme pools. Transcriptome and GO analyses identified two candidate genes related to auxin synthesis, transport, and signal transduction that were obviously down-regulated in the mutant. *BnARF16* is involved in auxin signal transduction, and *BnSIP3* is involved in the regulation of PAT. Through qRT-PCR analysis and transcriptome analysis, this study determined *BnSIP3* as the leading candidate gene, worth further investigation in rapeseed.

Analysis of the *Arabidopsis* homolog showed that *BnSIP3* encodes a CBL-interacting protein kinase. *BnSIP3* plays an important role in calcium regulation, salt stress and abscisic acid response pathways, root growth, and auxin transport (Chen et al., 2012; Held et al., 2011; Tripathi et al., 2009). The taproot growth rate and the rate of lateral root formation of the *Arabidopsis* homozygous *AtCIPK6* knockout line were extremely reduced, and this line also showed a reduction in auxin transport in the root apex and stem apex, indicating that AtCIPK6 participates in PAT (Tripathi et al., 2009). The *Atcipk6* mutant also showed a reduced root tip base and reduced stem-to-root apical auxin transport. The relative auxin transport rate and root phenotype of this mutant were similar to those of *pgp4-1* mutants which encodes an ABC integrated membrane transporter and plays a role in PAT. These observations strengthen our earlier proposal that CIPK6 is probably involved in PAT and indicate that it may function through the PGP4 auxin transporter. The study proposes that abnormal PAT is involved in stem bending in rapeseed (Fig. 6b). In the meristem region, an energy-dependent transport mechanism is needed to overcome the localized high auxin concentration gradient. When CIPK6 and PINs are co-localized subcellularly, the synergism of PIN–CIPK6 increases the rate and specificity of auxin transport and produces directional bias to auxin movement.

5. Conclusions

In this work, a *stb1* mutant with abnormal stem development of

rapeseed was found, the key stage of the stem bending occurred at the BBCH stages 59–61. Through genetic analysis and QTL mapping, identifying the *stb1* is controlled by a single recessive locus and the candidate interval was located between Bn-A01-p2421445 and Bn-A01-p4230829 on chromosome A01. In addition, this finding speculated that the phenotype of *stb1* may be caused by PAT through performing phenotype analysis and transcriptome analysis, the *BnSIP3* was determined as the most promising candidate gene within the QTL region. The synergism of PIN-CIPK6 increases the rate and specificity of auxin transport and produces directional bias to auxin movement. These results provide valuable insight into the molecular mechanisms controlling stem development and will aid breeding programs to improve stem strength and thus reduce the risk of yield loss due to lodging in rapeseed.

CRediT authorship contribution statement

Jiana Li: Conceptualization, Methodology, Funding acquisition.
Kun Lu: Conceptualization, Methodology, Funding acquisition, Writing – review & editing. **Mengna Yu:** Performed the sampling and experiments, Writing – original draft. **Rui Zhang:** Performed the sampling and experiments, Writing – original draft. **Yajun Liu:** Collected the phenotypes and performed the data analysis. **Yuan Gu:** Collected the phenotypes and performed the data analysis. **Guoxia Shang:** Collected the phenotypes and performed the data analysis. **Shengting Li:** Collected the phenotypes and performed the data analysis. **Yonghai Fan:** Software. **Miao Liu:** Validation. **Chuanfang Wan:** Validation. **Xuli Wu:** Validation. **Yuqiao Tang:** Validation. **Cunmin Qu:** Supervision. All authors have read and approved the manuscript.

Declaration of Competing Interest

The authors declare that they have no known competing financial interests or personal relationships that could have appeared to influence the work reported in this paper.

Acknowledgments

This work was supported by grants from the National Natural Science Foundation of China (31571701), the Talent Project of Chongqing Natural Science Foundation (cstc2021ycjh-bgzxm0033) the National Training Program of Innovation and Entrepreneurship for Undergraduates (202110635099), Chongqing Postgraduate Research Innovation Project (CYB21115), and Germplasm Creation Special Program of Southwest University.

Appendix A. Supporting information

Supplementary data associated with this article can be found in the online version at [doi:10.1016/j.indcrop.2021.114456](https://doi.org/10.1016/j.indcrop.2021.114456).

References

- Abas, L., Benjamins, R., Malenica, N., Paciorek, T., Wirniewska, J., Moulinier-Anzola, J.C., Sieberer, T., Friml, J., Luschnig, C., 2006. Intracellular trafficking and proteolysis of the *Arabidopsis* auxin-efflux facilitator PIN2 are involved in root gravitropism. *Nat. Cell Biol.* 8, 249–256. <https://doi.org/10.1038/ncb1369>.
- Barbez, E., Kubes, M., Rolcik, J., Beziat, C., Pencik, A., Wang, B., Rosquete, M.R., Zhu, J., Dobrev, P.I., Lee, Y., Zazimalova, E., Petrasek, J., Geisler, M., Friml, J., Kleine-Vehn, J., 2012. A novel putative auxin carrier family regulates intracellular auxin homeostasis in plants. *Nature* 485, 119–155. <https://doi.org/10.1038/nature11001>.
- Barbosa, I.C.R., Hammes, U.Z., Schwechheimer, C., 2018. Activation and polarity control of PIN-FORMED auxin transporters by phosphorylation. *Trends Plant Sci.* 23, 523–538. <https://doi.org/10.1016/j.tplants.2018.03.009>.
- Barrett, J.C., Fry, B., Maller, J., Daly, M.J., 2005. Haploview: analysis and visualization of LD and haplotype maps. *Bioinformatics* 15, 263–265. <https://doi.org/10.1093/bioinformatics/bth457>.
- Benkova, E., Michniewicz, M., Sauer, M., Teichmann, T., Seifertova, D., Jurgens, G., Friml, J., 2003. Local, efflux-dependent auxin gradients as a common module for plant organ formation. *Cell* 115, 591–602. [https://doi.org/10.1016/s0092-8674\(03\)00924-3](https://doi.org/10.1016/s0092-8674(03)00924-3).
- Bennett, M.J., Marchant, A., Green, H.G., May, S.T., Ward, S.P., Millner, P.A., Walker, A.R., Schulz, B., Feldmann, K.A., 1996. *Arabidopsis AUX1* gene: a permease-like regulator of root gravitropism. *Science* 273, 948–950. <https://doi.org/10.1126/science.273.5277.948>.
- Boerma, H.R., Jones, B.G., 1978. Inheritance of a second gene for brachytic stem in soybeans. *Crop Sci.* 18, 559–560. <https://doi.org/10.2135/cropsci1978.0011183x001800040008x>.
- Bu, D.C., Luo, H.T., Huo, P.P., Wang, Z.H., Zhang, S., He, Z.H., Wu, Y., Zhao, L.H., Liu, J.J., Guo, J.C., Fang, S.S., Cao, W.C., Yi, L., Yi Zhao, Y., Kong, L., 2021. KOBAS-i: intelligent prioritization and exploratory visualization of biological functions for gene enrichment analysis. *Nucleic Acids Res.* 49, W317–W325. <https://doi.org/10.1093/nar/gkab447>.
- Chalhoub, B., Denoeud, F., Liu, S., Parkin, I.A.P., Tang, H., Wang, X., Chiquet, J., Belcram, H., Tong, C., Samans, B., Correa, M., Da Silva, C., Just, J., Faletin, C., Koh, C.S., Le Clainche, I., Bernard, M., Bento, P., Noel, B., Labadie, K., Alberti, A., Charles, M., Arnaud, D., Guo, H., Daviaud, C., Alamyeri, S., Jabbari, K., Zhao, M., Edger, P.P., Chelaifa, H., Tack, D., Lassalle, G., Mestiri, I., Schnell, N., Le Paslier, M.C., Fan, G., Renault, V., Bayer, P.E., Golicz, A.A., Manoli, S., Lee, T.-H., Vinh Ha Dinh, T., Chalabi, S., Hu, Q., Fan, C., Tollenaere, R., Lu, Y., Battail, C., Shen, J., Sidebottom, C.H.D., Wang, X., Canaguier, A., Chauveau, A., Berard, A., Deniot, G., Guan, M., Liu, Z., Sun, F., Lim, Y.P., Lyons, E., Town, C.D., Bancroft, I., Wang, X., Meng, J., Ma, J., Pires, J.C., King, G.J., Brunel, D., Delourme, R., Renard, M., Aury, J.-M., Adams, K.L., Batley, J., Snowdon, R.J., Tost, J., Edwards, D., Zhou, Y., Hua, W., Sharpe, A.G., Paterson, A.H., Guan, C., Wincker, P., 2014. Early allopolyploid evolution in the post-Neolithic *Brassica napus* oilseed genome. *Science* 345, 950–953. <https://doi.org/10.1126/science.1253435>.
- Chen, L., Ren, F., Zhou, L., Wang, Q.Q., Zhong, H., Li, X.B., 2012. The *Brassica napus* Calcineurin B-Like 1/CBL-interacting protein kinase 6 (CBL1/CIPK6) component is involved in the plant response to abiotic stress and ABA signalling. *J. Exp. Bot.* 63, 6211–6222. <https://doi.org/10.1093/jxb/ers273>.
- Chen, S., Zhou, Y.Q., Chen, Y., Gu, J., 2018. Fastp: an ultra-fast all-in-one FASTQ preprocessor. *Bioinformatics* 34, i884–i890. <https://doi.org/10.1093/bioinformatics/bty560>.
- Dobin, A., Davis, C.A., Schlesinger, F., Drenkow, J., Zaleski, C., Jha, S., Batut, P., Chaisson, M., Gingeras, T.R., 2013. STAR: ultrafast universal RNA-seq aligner. *Bioinformatics* 29, 15–21. <https://doi.org/10.1093/bioinformatics/bts635>.
- Friml, J., 2003. Auxin transport - shaping the plant. *Curr. Opin. Plant Biol.* 6, 7–12. <https://doi.org/10.1016/s1369526602000031>.
- Friml, J., Wisniewska, J., Benkova, E., Mendgen, K., Palme, K., 2002. Lateral relocation of auxin efflux regulator PIN3 mediates tropism in *Arabidopsis*. *Nature* 415, 806–809. <https://doi.org/10.1038/415806a>.
- Galweiler, L., Guan, C.H., Muller, A., Wisman, E., Mendgen, K., Yephremov, A., Palme, K., 1998. Regulation of polar auxin transport by AtPIN1 in *Arabidopsis* vascular tissue. *Science* 282, 2226–2230. <https://doi.org/10.1126/science.282.5397.2226>.
- Geisler, M., Aryal, B., di Donato, M., Hao, P., 2017. A critical view on ABC transporters and their interacting partners in auxin transport. *Plant Cell Physiol.* 58, 1601–1614. <https://doi.org/10.1093/pcp/pcx104>.
- Geldner, N., Friml, J., Stierhof, Y.D., Jurgens, G., Palme, K., 2001. Auxin transport inhibitors block PIN1 cycling and vesicle trafficking. *Nature* 413, 425–428. <https://doi.org/10.1038/35096571>.
- Ginestet, C., 2011. ggplot2: elegant graphics for data analysis. *J. R. Stat. Soc. A Stat.* 174 https://doi.org/10.1111/j.1467-985X.2010.00676_9.x (245–245).
- Habets, M.E.J., Offringa, R., 2014. PIN-driven polar auxin transport in plant developmental plasticity: a key target for environmental and endogenous signals. *New Phytol.* 203, 362–377. <https://doi.org/10.1111/nph.12831>.
- Hashiguchi, Y., Niihama, M., Takahashi, T., Saito, C., Nakano, A., Tasaka, M., Morita, M.T., 2010. Loss-of-function mutations of retromer large subunit genes suppress the phenotype of an *Arabidopsis* zig mutant that lacks Qb-SNARE VTI11. *Plant Cell* 22, 159–172. <https://doi.org/10.1105/tpc.109.069294>.
- Held, K., Pascaud, F., Eckert, C., Gajdanowicz, P., Hashimoto, K., Corratge-Faillie, C., Offenborn, J.N., Lacombe, B., Dreyer, I., Thibaud, J.-B., Kudla, J., 2011. Calcium-dependent modulation and plasma membrane targeting of the AKT2 potassium channel by the CBL4/CIPK6 calcium sensor/protein kinase complex. *Cell Res.* 21, 1116–1130. <https://doi.org/10.1038/cr.2011.50>.
- Hoyerova, K., Hosek, P., Quareshy, M., Li, J., Klima, P., Kubes, M., Yemm, A.A., Neve, P., Tripathi, A., Bennett, M.J., Napier, R.M., 2018. Auxin molecular field maps define AUX1 selectivity: many auxin herbicides are not substrates. *New Phytol.* 217, 1625–1639. <https://doi.org/10.1111/nph.14950>.
- Kaneda, M., Schuetz, M., Lin, B.S.P., Chanis, C., Hamberger, B., Western, T.L., Ehling, J., Samuels, A.L., 2011. ABC transporters coordinately expressed during lignification of *Arabidopsis* stems include a set of ABCBs associated with auxin transport. *J. Exp. Bot.* 62, 2063–2077. <https://doi.org/10.1093/jxb/erq416>.
- Kato, T., Morita, M.T., Fukaki, H., Yamachi, Y., Uehara, M., Niihama, M., Tasaka, M., 2002. SGR2, a phospholipase-like protein, and ZIG/SGR4, a SNARE, are involved in the shoot gravitropism of *Arabidopsis*. *Plant Cell* 14, 33–46. <https://doi.org/10.1105/tpc.010215>.
- Khush, G.S., 2001. Green revolution: the way forward. *Nat. Rev. Genet.* 2, 815–822. <https://doi.org/10.1038/35093585>.
- Kilen, T.C., 1990. Brachytic stem and narrow leaflet effects on soybean seed composition and yield. *Crop Sci.* 30, 1006–1008. <https://doi.org/10.2135/cropsci1990.0011183x003000050010x>.
- Kilen, T.C., Hartwig, E.E., 1975. Short internode character in soybeans and its inheritance. *Crop Sci.* 15 <https://doi.org/10.2135/cropsci1975.0011183x001500060043x> (878–878).

- Lancashire, P.D., Bleiholder, H., Vandenboom, T., Langeluddeke, P., Stauss, R., Weber, E., Witzenberger, A., 1991. A uniform decimal code for growth-stages of crops and weeds. *Ann. Appl. Biol.* 119, 561–601. <https://doi.org/10.1111/j.1744-7348.1991.tb04895.x>.
- Lander, E.S., Green, P., Abrahamson, J., Barlow, A., Daly, M.J., Lincoln, S.E., Newberg, L.A., 1987. MAPMAKER: an interactive computer package for constructing primary genetic linkage maps of experimental and natural populations. *Genomics* 1, 174–181. [https://doi.org/10.1016/0888-7543\(87\)90010-3](https://doi.org/10.1016/0888-7543(87)90010-3).
- Lima, D.M., Linhares, T.S., Linares Lima, S.N., Carvalho, E.M., Loguerio, A.D., Bauer, J., Carvalho, C.N., 2019. Effect of sonic application of self-adhesive resin cements on push-out bond strength of glass fiber posts to root dentin. *Materials* 12, 1930. <https://doi.org/10.3390/ma12121930>.
- Liu, M., Chang, W., Yu, M.N., Fan, Y.H., Shang, G.X., Xu, Y.F., Niu, Y., Liu, X.M., Zhu, H., Dai, L.S., Tang, Z.L., Zhang, K., Liu, L.Z., Qu, C.M., Li, J.N., Lu, K., 2021. Overexpression of *DEFECTIVE IN ANTER DEHISCENCE 1* increases rapeseed siliques length through crosstalk between JA and auxin signaling. *Ind. Crop. Prod.* 168, 113576 <https://doi.org/10.1016/j.indcrop.2021.113576>.
- Ljung, K., Bhalerao, R.P., Sandberg, G., 2001. Sites and homeostatic control of auxin biosynthesis in *Arabidopsis* during vegetative growth. *Plant J.* 28, 465–474. <https://doi.org/10.1046/j.1365-313X.2001.01173.x>.
- Love, M.I., Huber, W., Anders, S., 2014. Moderated estimation of fold change and dispersion for RNA-seq data with DESeq2. *Genome Biol.* 15, 550. <https://doi.org/10.1186/s13059-014-0550-8>.
- Lu, K., Chai, Y.R., Zhang, K., Wang, R., Chen, L., Lei, B., Lu, J., Xu, X.F., Li, J.N., 2008. Cloning and characterization of phosphorus starvation inducible *Brassica napus PURPLE ACID PHOSPHATASE 12* gene family, and imprinting of a recently evolved MITE-minisatellite twin structure. *Theor. Appl. Genet.* 117, 963–975. <https://doi.org/10.1007/s00122-008-0836-x>.
- Lu, K., Li, T., He, J., Chang, W., Zhang, R., Liu, M., Yu, M.N., Fan, Y.H., Ma, J.Q., Sun, W., Qu, C.M., Liu, L.Z., Li, N.N., Liang, Y., Wang, R., Qian, W., Tang, Z.L., Xu, X.F., Lei, B., Zhang, K., Li, J.N., 2018. qPrimerDB: a thermodynamics-based gene-specific qPCR primer database for 147 organisms. *Nucleic Acids Res.* 46, D1229–D1236. <https://doi.org/10.1093/nar/gkx725>.
- Lu, K., Xiao, Z.C., Jian, H.J., Peng, L., Qu, C.M., Fu, M.L., He, B., Tie, L.M., Liang, Y., Xu, X.F., Li, J.N., 2016. A combination of genome-wide association and transcriptome analysis reveals candidate genes controlling harvest index-related traits in *Brassica napus*. *Sci. Rep.* 4, 636452. <https://doi.org/10.1038/srep36452>.
- Multani, D.S., Briggs, S.P., Chamberlin, M.A., Blakeslee, J.J., Murphy, A.S., Johal, G.S., 2003. Loss of an MDR transporter in compact stalks of maize *br2* and sorghum *dw3* mutants. *Science* 302, 81–84. <https://doi.org/10.1126/science.1086072>.
- Naramoto, S., 2017. Polar transport in plants mediated by membrane transporters: focus on mechanisms of polar auxin transport. *Curr. Opin. Plant Biol.* 40, 8–14. <https://doi.org/10.1016/j.pbi.2017.06.012>.
- Niu, Y., Wu, L.M., Li, Y.H., Huang, H.L., Qian, M.C., Sun, W., Zhu, H., Xu, Y.F., Fan, Y.H., Mahmood, U., Xu, B.B., Zhang, K., Qu, C.M., Li, J.N., Lu, K., 2020. Deciphering the transcriptional regulatory networks that control size, color, and oil content in *Brassica rapa* seeds. *Biotechnol. Biofuels* 13, 90. <https://doi.org/10.1186/s13068-020-01728-6>.
- Noh, B., Bandyopadhyay, A., Peer, W.A., Spalding, E.P., Murphy, A.S., 2003. Enhanced gravi- and phototropism in plant *mdr* mutants mislocalizing the auxin efflux protein PIN1. *Nature* 423, 999–1002. <https://doi.org/10.1038/nature01716>.
- Okada, K., Ueda, J., Komaki, M.K., Bell, C.J., Shimura, Y., 1991. Requirement of the auxin polar transport-system in early stages of *Arabidopsis* floral bud formation. *Plant Cell* 3, 677–684. <https://doi.org/10.1105/tpc.3.7.677>.
- Peng, J.R., Richards, D.E., Hartley, N.M., Murphy, G.P., Devos, K.M., Flintham, J.E., Beales, J., Fish, L.J., Worland, A.J., Pelica, F., Sudhakar, D., Christou, P., Snape, J. W., Gale, M.D., Harberd, N.P., 1999. ‘Green revolution’ genes encode mutant gibberellin response modulators. *Nature* 400, 256–261. <https://doi.org/10.1038/22307>.
- Pilu, R., Cassani, E., Villa, D., Curiale, S., Panzeri, D., Cerino Badone, F., Landoni, M., 2007. Isolation and characterization of a new mutant allele of *brachytic 2* maize gene. *Mol. Breed.* 20, 83–91. <https://doi.org/10.1007/s11032-006-9073-7>.
- Pnueli, L., Carmel-Goren, L., Hareven, D., Gutfinger, T., Alvarez, J., Ganal, M., Zamir, D., Lifschitz, E., 1998. The *SELF-PRUNING* gene of tomato regulates vegetative to reproductive switching of sympodial meristems and is the ortholog of *CEN* and *TFL1*. *Development* 125, 1979–1989. <https://doi.org/10.1242/dev.125.11.1979>.
- Rolando, C., Monties, B., LaPierre, C., 1992. Thioacidolysis. *Methods in Lignin Chemistry*. Springer-Verlag, Berlin, pp. 334–349.
- Stam, 1993. Construction of integrated genetic linkage maps by means of a new computer package: JoinMap. *Plant J.* 3, 739–744 <http://10.1111/j.1365-313X.1993.00739.x>.
- Swarup, R., Peret, B., 2012. AUX/LAX family of auxin influx carriers—an overview. *Front. Plant Sci.* 18, 225. <https://doi.org/10.3389/fpls.2012.00225>.
- Tripathi, V., Syed, N., Laxmi, A., Chattopadhyay, D., 2009. Role of CIPK6 in root growth and auxin transport. *Plant Signal. Behav.* 4, 663–665. <https://doi.org/10.4161/psb.4.7.9002>.
- Walker, D.B., Boerma, H.R., 1978. Morphological study of mechanism causing brachytic stem in soybeans. *Can. J. Plant Sci.* 58, 993–998. <https://doi.org/10.4141/cjps78-152>.
- Wang, B.H., Wi, Y.T., Huang, N.T., Zhu, X.F., Guo, W.Z., Zhang, T.Z., 2006. QTL mapping for plant architecture traits in upland cotton using RILs and SSR markers. *Acta Genet. Sin.* 33, 161–170. [https://doi.org/10.1016/s0379-4172\(06\)60035-8](https://doi.org/10.1016/s0379-4172(06)60035-8).
- Williams, M., Lowndes, L., Regan, S., Beardmore, T., 2015. Overexpression of *CYCD1;2* in activation-tagged *Populus tremula* × *Populus alba* results in decreased cell size and altered leaf morphology. *Tree Genet. Genomes* 11, 66. <https://doi.org/10.1007/s11295-015-0895-5>.
- Wu, S.Y., Xie, Y.R., Zhang, J.J., Ren, Y.L., Zhang, X., Wang, J.L., Guo, X.P., Wu, F.Q., Sheng, P.K., Wang, J., Wu, C.Y., Wang, H.Y., Huang, S.J., Wan, J.M., 2015. *VLN2* regulates plant architecture by affecting microfilament dynamics and polar auxin transport in rice. *Plant Cell* 27, 2829–2845. <https://doi.org/10.1105/tpc.15.00581>.
- Yang, L., Gordon, K.S., Wei, S., 2014. FeatureCounts: an efficient general-purpose program for assigning sequence reads to genomic features. *Bioinformatics* 30, 923–930. <https://doi.org/10.1093/bioinformatics/btt656>.
- Zheng, T.C., Li, L.L., Zhang, Q.X., 2018. Advances in research on tortuous traits of plants. *Euphytica* 214, 224. <https://doi.org/10.1007/s10681-018-2306-0>.